# ULTRA-BROADBAND HIGH-DIRECTIVITY DIRECTIONAL COUPLER DESIGN

*Joel D. Bickford* * + *G. R. Branner* + x

* *Hewlett-Packard Company, Santa Rosa, California*
\+ *University of California, Davis; Davis, California*
x *Avantek Inc., Santa Clara, California*

*ABSTRACT*

This paper discusses the theory and design of ultra-broadband high-directivity tapered line directional couplers.

Causes of imperfect directivity are examined from both a theoretical and experimental standpoint. This includes the effects of non-unity VSWR terminations and internal connections, unequal even and odd mode velocities, and unequal even and odd mode attenuation constants.

Practical considerations in the modern design of asymmetrical tapered couplers are discussed. Such information is significant in the choice of structure, layout, and tolerances to achieve maximum directivity.

An example design is presented which displays a bandwidth that is believed to be approximately 1.7 octaves greater than any other coupler of comparable directivity.

## *1. INTRODUCTION*

Broadband high-directivity directional couplers are of considerable importance in the design of modern precision microwave instrumentation systems. The requisite bandwidth is typically obtained in many directional coupler designs by employing stepped discrete equal length coupling sections, each with a constant value of coupling; however, such designs provide a multiplicity of step discontinuities which cause error in coupling realization and degradation in directivity [1,2,3,4,5,6]. A fundamental motivation for developing directional coupler designs utilizing continuous tapers has been the possibility of improving the directivity. Asymmetric tapered line directional couplers were first reported in 1954 by B.M. Oliver [7]. Many subsequent designs have incorporated exponentially tapered lines [7,8], polynomial approximations [9] and the Klopfenstein taper [10].

The objective of this paper is to discuss the theory and design of ultra-broadband high-directivity asymmetric directional couplers. An emphasis is placed on the examination of the causes of imperfect directivity from a theoretical and experimental standpoint. This includes the effects of non-unity VSWR terminations and internal connections, unequal even and odd mode phase velocities, and unequal even and odd mode attenuation constants. Whereas past publications have primarily stressed the synthesis of coupling functions, this paper places an emphases on practical considerations in the modern design of asymmetrical tapered couplers. These results will be of assistance to a designer in selecting an appropriate structure, layout and tolerancing to achieve optimal performance.

## *2. IDEAL COUPLER WITH NON-IDEAL TERMINATIONS*

Figure 1 illustrates a first order model of a practical coupler for analysis of non-ideal terminating effects. This configuration, which is employed to develop expressions that reveal essential parameters for directivity maximization, is composed of a composite network consisting of an ideal directional coupler emdedded inside two-ports at each of its four terminals.

The imperfect transmission lines, connectors, dielectric support beads, transitions and other sources of external error which exist inside the terminals of a practical directional coupler are lumped into the two-port networks $N_1$-$N_4$. The terms $\Gamma_1$, $\Gamma_2$, $\Gamma_3$, and $\Gamma_4$ are the reflection coefficients seen by the ideal coupler due to the imperfections previously described. Since the area of concern in this paper is *high-directivity* couplers, we can make some initial assumptions about the quality of these external two-port networks. A reasonable amount of care in the design and manufacture of a precision coupler minimizes the effects of the external error sources represented by the networks $N_i$ where the VSWR's of the networks are less than 1.1 so that

$$\Gamma_i \ll 1 \tag{2.1}$$

The insertion loss of the two-ports $N_i$ are typically 0.15 dB or less so that negligible power is lost through the two-ports. Since we know that the embedded coupler itself is lossless and ideal, we know that

$$Zo = \sqrt{Zoe(x)\,Zoo(x)} \tag{2.2}$$

at all points along the length of the ideal coupler. Furthermore, with $[s]$ being the scattering matrix of the ideal coupler, we have the usual assumptions that $s_{ii}=0$, $[s]=[s]^T$, $s_{13}=s_{24}=0$, $|s_{12}|=|s_{34}|$, and $|s_{14}|=|s_{23}|$.

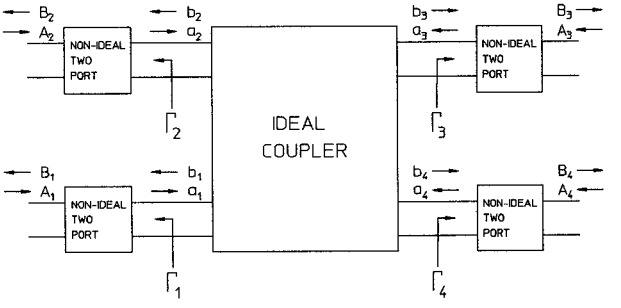


Figure 1. Ideal coupler with non-ideal two-ports

In Figure 1, we define the incident and reflected waves of the overall structure as $A_i$ and $B_i$ respectively at port $i$, and we define $a_i$ and $b_i$ as the incident and reflected waves at port $i$ of the "ideal" coupled line structure. To find the directivity of the overall structure, we define the coupling of the composite network as the ratio of the coupled to incident power ($|B_3|/|A_4|$ or, similarly, $|B_2|/|A_1|$), the isolation as the ratio of the power transmitted diagonally to the incident power ($|B_3|/|A_1|$ or, similarly, $|B_2|/|A_4|$), and the directivity as the ratio of coupling to isolation which is $|B_3/A_4|/|B_3/A_1|$.

To find the isolation ratio $|B_3/A_1|$, we inject a signal $A_1$ into port 1 and find the magnitude of signal $B_3$ out port 3 while the signals $A_2$, $A_3$ and $A_4$ are 0. Employing the previously stated assumptions yields [11]

$$\frac{b_3}{a_1} = \frac{s_{12}\Gamma_2 s_{23} + s_{14}\Gamma_4 s_{34}}{1 - s_{23}^2\Gamma_2\Gamma_3 - s_{34}^2\Gamma_3\Gamma_4} \approx \frac{B_3}{A_1} \tag{2.3}$$

Since we are assuming that the reflection coefficients presented to the coupler ($\Gamma_1$, $\Gamma_2$, $\Gamma_3$, $\Gamma_4$) are much less than 1, any term containing the product of two or more $\Gamma$ terms is often negligible. We can see that the second two terms in the denominator of 2.3 are much less than the first, and can therefore be ignored. This gives us the following result for the isolation



0149-645X/88/0000-0595$01.00 © 1988 IEEE

$$Isolation = \frac{B_3}{A_1} \approx s_{12}\Gamma_2 s_{23} + s_{14}\Gamma_4 s_{34} \tag{2.4}$$

This shows that the match presented to ports 2 and 4 ($\Gamma_2$ and $\Gamma_4$) have the most significant effect on the isolation.

As stated previously, the coupling is $|B_3|/|A_4|$. We now compute this parameter in order to arrive at the overall directivity. Proceeding in a similar manner as in the derivation of the isolation, we find the coupling to be [11]

$$\frac{b_3}{a_4} = \frac{s_{34} - s_{34}s_{12}^2\Gamma_1\Gamma_2 + s_{23}\Gamma_2 s_{12}\Gamma_1 s_{14}}{1 - s_{12}^2\Gamma_1\Gamma_2 - s_{23}^2\Gamma_3\Gamma_2} \approx \frac{B_3}{A_4} \tag{2.5}$$

The second factor in the numerator is smaller than the first by a factor of more than $\Gamma_1\Gamma_2$. Based on our previous assumptions, this term can be neglected. For the ideal coupler, we know that $|s_{12}| = |s_{34}|$, hence, it is also apparent that the third numerator term is also much smaller than the first. The numerator is therefore approximately $s_{34}$. Similar reasoning shows that the second and third terms in the denominator are much smaller than the first. The final result for the coupling is then

$$coupling = \frac{B_3}{A_4} \approx \frac{b_3}{a_4} \approx s_{34} \tag{2.6}$$

The conclusion may be drawn that the coupling is largely unaffected by small mismatches on any of the ports.

The directivity of the coupler (coupling/isolation) can be written from the expression for the isolation (2.5) and the coupling (2.6) as follows:

$$D \approx \frac{1}{s_{12}/s_{34}\Gamma_2 s_{23} + \Gamma_4 s_{14}} \tag{2.7}$$

In order to maximize this quantity, we must minimize the denominator. Since we know that $|s_{12}/s_{34}| = 1$ and that $|s_{23}| = |s_{14}|$, the denominator terms in equation 2.7 differ in magnitude only by the difference between $\Gamma_2$ and $\Gamma_4$. This means that the matches $\Gamma_2$ and $\Gamma_4$ are of *equal* importance in maximizing the directivity. The designer should therefore concentrate on developing a structure which optimizes the match at these two ports. Since $\Gamma_1$ and $\Gamma_3$ do not appear, they are far less important.

## *3. ASYMMETRICAL TAPERED DIRECTIONAL COUPLER THEORY*

In this section, a non-ideal asymmetrically-tapered coupler with ideal terminations on each of the coupler's four ports is analyzed, however, the method of analysis is easily applied to other types of couplers.

Expressions for coupling and directivity are derived based on an even mode and odd mode excitation analysis. Any excitation at ports 1 and 2 can be analyzed as a superposition of these two basic modes.

The asymmetrical tapered coupler to be analyzed is represented in Figure 2. The even and odd mode signal generators are shown at the left end of the coupler with their respective polarities. To the right of the generators are the source impedances $Z_o$. The tapered lines are a schematic representation of what the two conductors would look like in a structure such as edge-coupled stripline. At the far end are the port impedances $Z_l$.

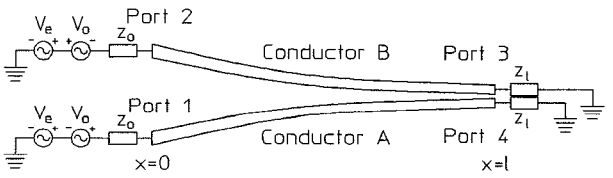


Figure 2. Asymmetrical tapered coupler

At the loosely coupled (left) end of the coupler, we ideally have $Z_{oe} = Z_{oo} = Z_o$, which is the characteristic impedance of the system. At the other end, we have $Z_{oe} > Z_o$ and $Z_{oo} < Z_o$. A designer usually attempts to maintain $Z_{oe}(x)Z_{oo}(x) = Zo^2$, however, that assumption will *not* be made for the following analysis.

Above some frequency, the slow variations of $Z_{oe}$ and $Z_{oo}$ with distance cause the coupled transmission lines to behave as nearly reflectionless transformers [12]. Reflections generated *within* the transformers tend to cancel each other to produce a very small net reflection. For most practical applications, if the taper function is properly chosen, the taper will perform well at frequencies where the taper length is longer than 0.2 to 0.5 wavelength [9]. If a small passband ripple is required, then the taper must be longer than that required for a larger passband ripple.

With reference to Figure 2, we may inject an even mode signal of value $\Psi$ into to ports 1 and 2. This gives

$$v_{Ae}^+(0) = \Psi, \qquad v_{Be}^+(0) = \Psi \tag{3.1}$$

where $v_{Ae}^+(0)$ and $v_{Be}^+(0)$ are the voltage waves traveling in the $+x$ direction at $x = 0$ on conductors A and B respectively while excited in the even mode.

The tapered lines behave as transformers causing the voltages and currents on the lines to maintain the ratio of $v_e^+(x)/i_e^+(x) = Z_{oe}(x)$ along the coupler. As the signal approaches $x = l$, we have on the coupled lines [11]

$$v_{Be}^+(l) = v_{Ae}^+(l) = \Psi\sqrt{Z_{oe}(l)/Z_o}\; e^{-(\alpha_e + j\beta_e)l} \tag{3.2}$$

where $\alpha_e$ and $\beta_e$ are the effective attenuation and phase constants such that $\beta_e l$ is the overall even mode delay and $\alpha_e l$ is the overall even mode loss.

Since the load $Z_l$ is not equal to the even mode impedance at ports 3 and 4, the wave has transmitted and reflected components. The reflection coefficient at the load is

$$\Gamma_{le} = \frac{Z_l - Z_{oe}(l)}{Z_l + Z_{oe}(l)} \tag{3.3}$$

The reflected signals from ports 3 and 4 are therefore

$$v_{Be}^-(l) = v_{Ae}^-(l) = \Psi e^{-(\alpha_e + j\beta_e)l}\left(\frac{Z_l - Z_{oe}(l)}{Z_l + Z_{oe}(l)}\right)\sqrt{Z_{oe}(l)/Z_o} \tag{3.4}$$

The voltages resulting at ports 3 and 4 are

$$V4_e = V3_e = v_{Be}^-(l) + v_{Be}^+(l) = v_{Be}^+(l)(1 + \Gamma_{le}) \tag{3.5}$$

or

$$V4_e = V3_e = \Psi e^{-(\alpha_e + j\beta_e)l}\left(1 + \frac{Z_l - Z_{oe}(l)}{Z_l + Z_{oe}(l)}\right)\sqrt{Z_{oe}(l)/Z_o} \tag{3.6}$$

A similar analysis performed for the odd mode yields:

$$V4_o = -V3_o = \Psi e^{-(\alpha_o + j\beta_o)l}\left(1 + \frac{Z_l - Z_{oo}(l)}{Z_l + Z_{oo}(l)}\right)\sqrt{Z_{oo}(l)/Z_o} \tag{3.7}$$

The reflected waves for the even and odd modes travel back down the coupler to $x = 0$. At this point in the ideal coupler, $Z_{oe}(0) = Z_{oo}(0) = Z_o$. Since the characteristic impedance of each mode is equal to the source impedance, there is no reflection and the signals are completely absorbed.

Since we are analyzing a linear system, we may excite the coupler in the even and odd modes simultaneously and the resulting voltages and currents on the coupler are found by linear superposition.

At ports 1 and 2 the resulting incident voltages are

$$v_A^+(0) = v_{Ae}^+(0) + v_{Ao}^+(0) = 2\Psi \tag{3.8}$$

$$v_B^+(0) = v_{Be}^+(0) + v_{Bo}^+(0) = 0 \tag{3.9}$$

Note that with this excitation, there is no incident signal at port 2, and there is a $2\Psi$ signal at port 1. This example is equivalent to the case when the coupler is excited from port 1 only by a single generator.

The voltage at port 4 is the signal transmitted through the main arm of the coupler. Its voltage is

$$V4 = V4_e + V4_o \tag{3.10}$$

or

$$V4=\Psi e^{-(\alpha_e+j\beta_e)l}\left(1+\frac{Z_l-Z_{oe}(l)}{Z_l+Z_{oe}(l)}\right)\sqrt{Z_{oe}(l)/Z_o}$$

$$+\ \Psi e^{-(\alpha_o+j\beta_o)l}\left(1+\frac{Z_l-Z_{oo}(l)}{Z_l+Z_{oo}(l)}\right)\sqrt{Z_{oo}(l)/Z_o} \qquad (3.11)$$

The voltage at port 3 is similarly found to be

$$V3=\Psi e^{-(\alpha_e+j\beta_e)l}\left(1+\frac{Z_l-Z_{oe}(l)}{Z_l+Z_{oe}(l)}\right)\sqrt{Z_{oe}(l)/Z_o}$$

$$-\ \Psi e^{-(\alpha_o+j\beta_o)l}\left(1+\frac{Z_l-Z_{oo}(l)}{Z_l+Z_{oo}(l)}\right)\sqrt{Z_{oo}(l)/Z_o} \qquad (3.12)$$

From the definition of scattering parameters and equations 3.8 and 3.9 we can show that

$$a_1=\frac{v_A^+(0)}{\sqrt{Z_o}}=\frac{2\Psi}{\sqrt{Z_o}} \qquad a_2=0 \qquad (3.13)$$

Similarly, we can show that $b_3=V3/\sqrt{Z_l}$ if $Z_l$ is real [13]. The isolation for this case is

$$\frac{b_3}{a_1}=\frac{1}{2}\sqrt{Z_o/Z_l}\,e^{-(\alpha_e+j\beta_e)l}\left(1+\frac{Z_l-Z_{oe}(l)}{Z_l+Z_{oe}(l)}\right)\sqrt{Z_{oe}(l)/Z_o}$$

$$-\ \frac{1}{2}\sqrt{Z_o/Z_l}\,e^{-(\alpha_o+j\beta_o)l}\left(1+\frac{Z_l-Z_{oo}(l)}{Z_l+Z_{oo}(l)}\right)\sqrt{Z_{oo}(l)/Z_o} \qquad (3.14)$$

In order to achieve perfect isolation from port 1 to port 3, Equation 3.14 must equal 0 for all frequencies. We must therefore have $\alpha_e=\alpha_o$, $\beta_e=\beta_o$, and the remaining requirements that

$$\sqrt{Z_{oe}(l)/Z_o}\left(1+\frac{Z_l-Z_{oe}(l)}{Z_l+Z_{oe}(l)}\right)=\sqrt{Z_{oo}(l)/Z_o}\left(1+\frac{Z_l-Z_{oo}(l)}{Z_l+Z_{oo}(l)}\right) \qquad (3.15)$$

Equation 3.15 is met if and only if

$$Z_l=\sqrt{Z_{oe}(l)Z_{oo}(l)} \qquad (3.16)$$

Note that this termination value is independent of the generator impedance $Z_o$. This important result shows that the directional coupler can simultaneously act as an impedance transformer.

It is important to note that if $Z_l=\sqrt{Z_{oe}(l)Z_{oo}(l)}$, $\alpha_e\neq\alpha_o$, or especially $\beta_e\neq\beta_o$, then the isolation and directivity will be affected. The expression for isolation, equation 3.14, may then be employed as a measure of degradation.

Now that we have determined the conditions for isolation from port 1 to port 3, the coupling from port 4 to 3 is desired.

If we drive ports 3 and 4 in the even mode, the signal experiences a reflection as it enters the coupled line structure at $x=l$. The reflection coefficient is

$$\rho_e=\frac{Z_{oe}(l)-Z_l}{Z_{oe}(l)+Z_l} \qquad (3.17)$$

Similarly, for the odd mode

$$\rho_o=\frac{Z_{oo}(l)-Z_l}{Z_{oo}(l)+Z_l} \qquad (3.18)$$

Again, exciting the structure in the even and odd mode simultaneously from ports 3 and 4 and employing superposition, the coupling to port 3 will be $b_3/a_4$ or

$$\frac{b_3}{a_4}=s_{34}=\frac{\Psi}{2\Psi}(\rho_e-\rho_o)=\frac{1}{2}(\rho_e-\rho_o) \qquad (3.19)$$

If $Z_l=\sqrt{Z_{oe}(l)Z_{oo}(l)}$ (which was required for perfect isolation) then

$$\rho_e=-\rho_o \qquad (3.20)$$

and from 3.19

$$s_{34}=\rho_e \qquad (3.21)$$

If we assume that $Z_l=Z_o=\sqrt{Z_{oe}(l)Z_{oo}(l)}$ then the coupling between ports 1 and 2 is

$$s_{12}=s_{21}=\left(\rho_o e^{-2(\alpha_o+j\beta_o)l}-\rho_e e^{-2(\alpha_e+j\beta_e)l}\right) \qquad (3.22)$$

In a practical coupler there is some loss ($\alpha_e\neq 0$ and $\alpha_o\neq 0$) which means that $|s_{12}|<|s_{34}|$. This will cause the directivity to be better if port 3 (or 4) is chosen as the coupled port.

*4. EXAMPLE BROADBAND HIGH-DIRECTIVITY TAPERED COUPLER*

The physical structure of the prototype directional coupler, illustrated in Figure 3a, is constructed so that the two round conducting rods remain parallel throughout the coupling region. A septum with a tapered opening, as shown in Figure 3b, controls the amount of coupling between the rods along the coupler. The diameter of the rods is adjusted along the length to maintain a value of $Z_o$ of 50 ohms (Eq. 2.2). In order to obtain proper mechanical dimensions such as rod diameters, spacings and septum opening width, a special computer program is employed which is based on the computation of the solution of Laplace's equation in a 2-dimensional region in terms of an equivalent source [14].

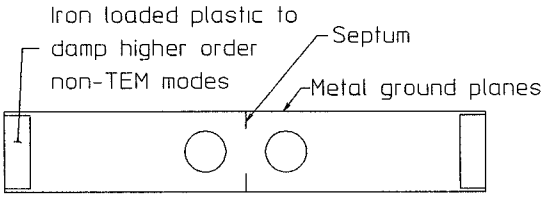


Figure 3A. Coupler cross section (not to scale)

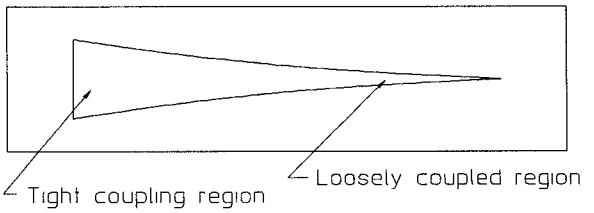


Figure 3B. Septum (not to scale)

In addition to its physical realization, the unique features of this device are its broad bandwidth and high directivity which were obtained utilizing a Klopfenstein [15] taper function. Although this taper provides an equal-ripple reflection coefficient for the case of a two-port transformer, it does not provide equal ripple coupling for a coupler. Although this might appear to violate Young's [16] equivalence principle, this is not the case. In the case of Klopfenstein's transformer, the taper is terminated in a load impedance $Z_l$ where $Z_l\neq Z_o$. In the coupler case, the taper is generally terminated with a load impedance $Z_l$ where $Z_l=Z_o$. This difference causes the coupling to overshoot at the low end of the frequency band as seen in Figure 5. If equal-ripple passband coupling is required, then Arndt's [9] taper should be used. We chose to use the Klopfenstein taper for the prototype coupler since it is is to be used down to 45 MHz and the coupling rolloff of his taper is less than Arndt's in that frequency range.

A photograph of the final directional coupler realization is shown in Figure 4. Some metal was removed and tuning screws were added to the center conductors and the ground planes at the point where the abrupt septum opening occurs. These adjustments were required to compensate for parasitics caused by the abruptly changing ground plane [11]. These

parasitic reactances at the tightly coupled end of the coupler can have a very adverse effect on the coupler directivity. While the reactances cause some mismatch reflection, the major problem is differential delay between the even and odd modes. This differential delay causes the isolation to be poor by changing the effective $\beta_e$ and $\beta_o$ in equation 3.13.

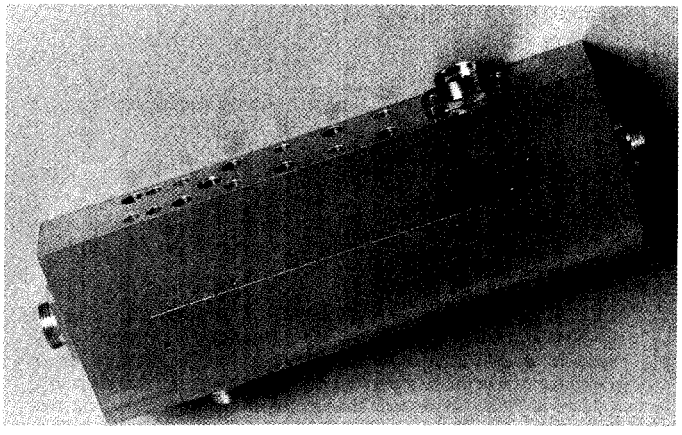

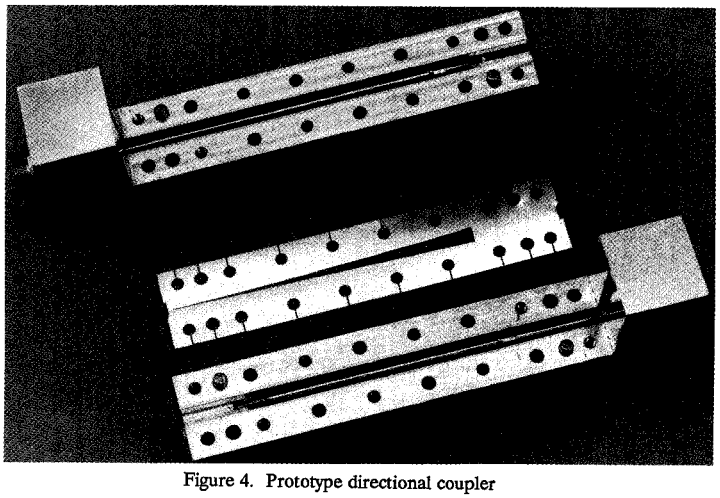

Figure 4. Prototype directional coupler

The performance of an example 27 dB directional coupler is illustrated in Figure 5. The data for this device indicates that up to 13 GHz, the worst case directivity is greater than 30 dB, and over the range between 13 and 18 GHz it exceeds 25 dB. The coupling is seen to be extremely flat over the entire 0.5 to 18 GHz frequency range with the exception of the expected overshoot at the lowest end of the band. In figure 5, the return loss is seen to be better than -25 dB up to 13 GHz, and better than -20 dB over the remainder of the band.

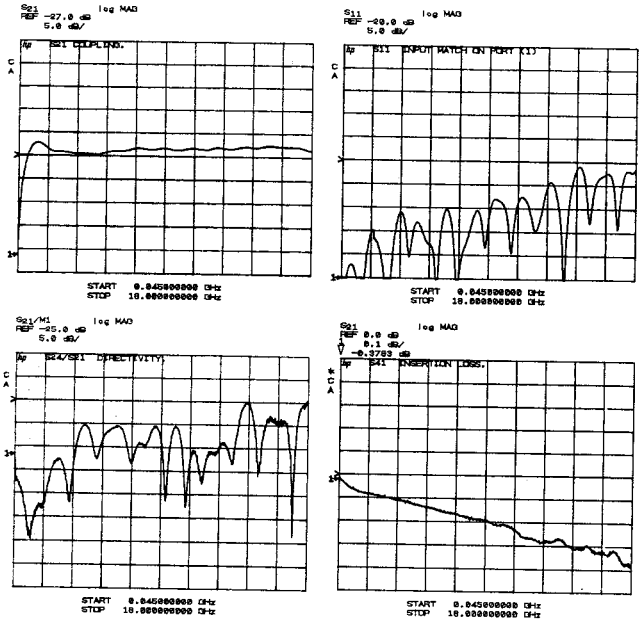

Figure 5. Prototype coupler performance


*References*

[1] J. K. Shimizu and E. M. T. Jones "Coupled-Transmission-Line Directional Couplers," IRE Trans. on Microwave Theory and Techniques, October, 1958.

[2] E. G. Cristal and L. Young "Theory and Tables of Optimum Symmetrical TEM-Mode Coupled-Transmission-Line Directional Couplers," IEEE Trans. on Microwave Theory and Techniques, Vol. MTT-13, No. 5, pp. 544-558, September 1965.

[3] R. Levy "General Synthesis of Asymmetric Multi-Element Coupled-Transmission-Line Directional Couplers," IEEE Trans. on Microwave Theory and Techniques, Vol. MTT-11, No. 4, pp. 226-237, July 1963.

[4] R. Levy "Tables for Asymmetric Multi-Element Coupled-Transmission-Line Directional Couplers," IEEE Trans. on Microwave Theory and Techniques, Vol. MTT-12, No. 3, pp. 275-279, May 1964.

[5] J. P. Shelton and J. A. Mosko "Synthesis and Design of Wide-Band Equal-Ripple TEM Directional Couplers and Fixed Phase Shifters," IEEE Trans. on Microwave Theory and Techniques, Vol. MTT-14, No. 10, October 1966.

[6] Leo Young "Parallel Coupled Lines and Directional Couplers," Artech House Inc. 1972.

[7] B. M. Oliver, "Directional Electromagnetic Couplers," Proc. IRE, Vol. 42, No. 11, pp. 1686-1692, November 1954.

[8] S. Yamamoto, T. Azakami, and K. Itakura, "Coupled Nonuniform Transmission Line and Its Applications," IEEE Trans. on Microwave Theory and Techniques, Vol. MTT-15, No. 4, April 1967.

[9] F. Arndt "Tables for Asymmetric Chebyshev High-Pass TEM-Mode Directional Couplers," IEEE Trans. on Microwave Theory and Techniques, Vol. MTT-18, No. 9, pp. 633-638, September 1970.

[10] R. H. DuHamel and M. E. Armstrong "The Tapered-Line Magic-T" A Wide-Band Monopulse Antenna, Abstracts of the Fifteenth Annual Symposium on the USAF Antenna Research and Development Program, Monticello, Illinois, October 1965.

[11] J. D. Bickford "Broadband High-Directivity TEM Directional Coupler Design," Masters Thesis, University of California at Davis. To be published.

[12] R. E. Collin, "Foundations for Microwave Engineering" New York: McGraw- Hill, 1966.

[13] D. C. Youla, "Analysis and Synthesis of Arbitrarily Terminated Lossless Nonuniform Lines," IEEE Trans. on Circuit Theory, Vol. CT-11, pp. 363-372, September 1964.

[14] R. F. Harrington, K. Pontoppidan, P. Abrahamsen and N. C. Albertsen, "Computation of Laplacian Potentials by an Equivalent Source Method," Proc. IEEE, Vol. 116, No. 10, October 1969.

[15] R. W. Klopfenstein, "A Transmission Line Taper of Improved Design," Proc. IRE, Vol. 44, pp. 31-35, January 1956.

[16] Leo Young, "The Analytical Equivalence of TEM-Mode Directional Couplers and Transmission-Line stepped-impedance filters," Proc. IEEE, Vol 110, No. 2, February 1963.